Anisotropic magnetic, electrical, and thermal transport properties of the Y-Al-Ni-Co decagonal approximant

Ana Smontara, I. Smiljanić, J. Ivkov, D. Stanić, and O. S. Barišić
Laboratory for the Study of Transport Problems, Institute of Physics, Bijenička 46, P.O. Box 304, HR-10001 Zagreb, Croatia

Z. Jagličić
Institute of Mathematics, Physics and Mechanics, University of Ljubljana, Jadranska 19, SI-1000 Ljubljana, Slovenia

P. Gille
Department of Earth and Environmental Sciences, Crystallography Section, Ludwig-Maximilians-Universität München, Theresienstrasse 41, D-80333 München, Germany

M. Komelj, P. Jeglič, M. Bobnar, and J. Dolinšek
J. Stefan Institute, University of Ljubljana, Jamova 39, SI-1000 Ljubljana, Slovenia
(Received 19 March 2008; revised manuscript received 7 June 2008; published 16 September 2008)

We have investigated anisotropic physical properties (magnetic susceptibility, electrical resistivity, thermoelectric power, Hall coefficient, and thermal conductivity) of Y-Al-Ni-Co decagonal approximant with composition $Al_{76}Co_{22}Ni_2$. The crystalline-direction-dependent measurements were performed along three orthogonal directions a^*, b, and c of the Y-Al-Ni-Co unit cell, where (a,c) monoclinic atomic planes are stacked along the perpendicular b direction. Anisotropic magnetic susceptibility of conduction electrons is paramagnetic for the field lying within the (a,c) atomic planes and diamagnetic for the field along the b direction. Anisotropic electrical resistivity is low in all crystalline directions, appearing in the order $\rho_{a^*} > \rho_c \gg \rho_b$. Thermopower shows electron-phonon enhancement effect. Anisotropic bare thermopower (in the absence of electron-phonon interactions) was extracted, appearing in the same order as the resistivity, $|S^{\mathrm{bare}}_{a^*}/T| > |S^{\mathrm{bare}}_{c}/T| > |S^{\mathrm{bare}}_{b}/T|$. Anisotropic thermal conductivity appears in the order $\kappa^b > \kappa^c > \kappa^{a^*}$, so that b is the most conducting direction for both electricity and heat. Hall coefficient R_H exhibits pronounced anisotropy, where the magnetic field in a given crystalline direction yields the same R_H for the current along the other two crystalline directions in the perpendicular plane. These anisotropies are analyzed in terms of the anisotropic structure of the Y-Al-Ni-Co phase and the *ab initio* calculated anisotropic Fermi surface. The results are compared with the literature-reported anisotropy of the physical properties of the *d*-Al-Ni-Co decagonal quasicrystal.

DOI: 10.1103/PhysRevB.78.104204 PACS number(s): 61.44.Br, 71.23.Ft

I. INTRODUCTION

Decagonal quasicrystals (*d*-QCs) can be structurally viewed as a periodic stack of quasiperiodic atomic planes, so that *d*-QCs are two-dimensional (2D) quasicrystals, whereas they are periodic crystals in a direction perpendicular to the quasiperiodic planes. This duality makes *d*-QCs especially suitable to study the effect of quasiperiodicity on the physical properties of the material, as a given property can be investigated on the same sample along the quasiperiodic (Q) and periodic (P) directions. Literature reports reveal that *d*-QCs exhibit anisotropy in their electrical and thermal transport properties [electrical resistivity ρ,[1–3] thermoelectric power S,[4] Hall coefficient R_H,[5,6] thermal conductivity κ,[7,8] and optical conductivity $\sigma(\omega)$ (Ref. 9)] when measured along the Q and P directions. A striking example of the anisotropic nature of *d*-QCs is their electrical resistivity, which shows positive temperature coefficient (PTC) at metallic values along the P direction (e.g., $\rho_P^{300\ \mathrm{K}} \approx 40\ \mu\Omega\,\mathrm{cm}$ in *d*-Al-Cu-Co and *d*-Al-Ni-Co),[2] whereas the resistivity in the quasiperiodic plane is considerably larger (e.g., $\rho_Q^{300\ \mathrm{K}} \approx 330\ \mu\Omega\,\mathrm{cm}$) (Ref. 2) and exhibits a negative temperature coefficient (NTC) and sometimes also a maximum somewhere below room temperature (RT) or a leveling off upon $T \to 0$. The degree of anisotropy is related to the structural details of a particular decagonal phase, depending on the number of quasiperiodic layers in one periodic unit.[10,11] The most anisotropic case is the phases with just two layers, realized in *d*-Al-Ni-Co and *d*-Al-Cu-Co, where the periodicity length along the periodic axis is about 0.4 nm and the resistivity ratio at RT amounts typically $\rho_Q/\rho_P \approx 6-10$.[1–3] Other *d* phases contain more quasiperiodic layers in a periodic unit and show smaller anisotropies. In *d*-Al-Co, *d*-Al-Ni, and *d*-Al-Si-Cu-Co there are four quasiperiodic layers with periodicity of about 0.8 nm and the RT anisotropy is $\rho_Q/\rho_P \approx 2-4$.[4] *d*-Al-Mn, *d*-Al-Cr, and *d*-Al-Pd-Mn phases contain six layers with periodicity of about 1.2 nm and the anisotropy amounts $\rho_Q/\rho_P \approx 1.2-1.4$, whereas *d*-Al-Pd and *d*-Al-Cu-Fe phases with eight layers in a periodicity length of 1.6 nm are close to isotropic. The basic question here is whether the observed anisotropy is a consequence of the quasiperiodic structural order within the 2D atomic layers versus the periodic order in the perpendicular direction or the anisotropy is rather a consequence of complex local atomic order on the scale of near-neighbor atoms with no direct relationship to the quasiperiodicity.

While this question has so far not been answered satisfactorily for the *d*-QCs, the situation is clearer for approximants

of the decagonal phase. Approximant phases are characterized by large unit cells, which periodically repeat in space, but the structure of the unit cell closely resembles *d*-QCs. Atomic layers are again stacked periodically and the periodicity lengths along the stacking direction are almost identical to those along the periodic direction of *d*-QCs. Moreover, atomic planes of approximants and *d*-QCs show locally similar quasiperiodic patterns, so that their structures on the scale of near-neighbor atoms closely resemble each other. Decagonal approximants thus offer valid comparison of the physical properties to the *d*-QCs with the advantage that theoretical simulations for the approximants—being periodic solids—are straightforward to perform, whereas this is not the case for the nonperiodic *d*-QCs.

Recently, the anisotropic magnetic and transport properties (electrical resistivity, thermopower, Hall coefficient, and thermal conductivity), measured along three orthogonal crystalline directions, were reported for the $Al_4(Cr,Fe)$ complex metallic alloy with composition $Al_{80}Cr_{15}Fe_5$.[12,13] This compound belongs to the class of orthorhombic Al_4TM [transition-metal (TM)] phases first described by Deng *et al.*,[14] which are approximants to the decagonal phase with six atomic layers in a periodic unit of 1.25 nm and comprising about 306 atoms in the giant unit cell. The measurements showed that the in-plane electrical resistivity of this compound exhibits nonmetallic behavior with NTC and a maximum in $\rho(T)$, whereas the resistivity along the stacking direction shows PTC. The important conclusions were that the nonmetallic $\rho(T)$ occurs in the presence of a high density of charge carriers [there is no pseudogap in the electronic density of states (DOS) at the Fermi energy E_F] and the anisotropy of the resistivity along the three orthorhombic directions is a consequence of local atomic order on the scale of nearest-neighbor atoms, pertinent to the specific structure of the $Al_4(Cr,Fe)$ phase, with no direct relationship to the intermediate-scale quasiperiodic patterns in the structure. The resistivity in all three crystalline directions could be theoretically reproduced by a unified physical picture using the theory of slow charge carriers by Trambly de Laissardière *et al.*[15] Anisotropies in the electronic transport properties similar to those in *d*-QCs were also reported for the decagonal approximants $Al_{13}Co_4$, $Al_{13}Fe_4$, and the Taylor-phase Al_3Mn,[16] where the investigated samples were not single crystalline but showed morphology of oriented crystal bundles.

In this paper we report a study of the anisotropic physical properties (magnetic susceptibility, electrical resistivity, thermopower, Hall coefficient, and thermal conductivity) of a complex metallic alloy $Al_{13-x}(Co_{1-y}Ni_y)_4$, also known as the Y-Al-Ni-Co phase, which is a monoclinic approximant of the decagonal phase with two atomic layers within one periodic unit along the stacking direction and a relatively small unit cell, comprising 32 atoms. Due to the considerably smaller unit cell, the structure of Y-Al-Ni-Co is relatively simple as compared to the much higher complexity of the aforementioned $Al_4(Cr,Fe)$ phase with 306 atoms/unit cell. The measurements of the anisotropy in Y-Al-Ni-Co thus allow comparison of this simple decagonal approximant to the $Al_4(Cr,Fe)$ phase,[12,13] a decagonal approximant with a considerably higher structural complexity. Moreover, Y-Al-Ni-Co allows comparison to the closely related *d*-Al-Ni-Co quasicrystal, which is the main aim of this paper.

II. STRUCTURAL CONSIDERATIONS AND SAMPLE PREPARATION

The $Al_{13-x}(Co_{1-y}Ni_y)_4$ monoclinic phase[17] belongs to the $Al_{13}TM_4$ class of decagonal approximants. Other members are monoclinic $Al_{13}Co_4$,[18] orthorhombic $Al_{13}Co_4$,[19] monoclinic $Al_{13}Fe_4$,[20] monoclinic $Al_{13}Os_4$,[21] $Al_{13}Ru_4$ (isotypical to $Al_{13}Fe_4$),[22] and $Al_{13}Rh_4$ (also isotypical to $Al_{13}Fe_4$).[23] The structure of $Al_{13-x}(Co_{1-y}Ni_y)_4$ with $x=0.9$ and $y=0.12$, corresponding to composition $Al_{75}Co_{22}Ni_3$, was first described by Zhang *et al.*[17] Lattice parameters of the monoclinic unit cell [space group $C2/m$ (No. 12)] are $a=17.071(2)$ Å, $b=4.0993(6)$ Å, $c=7.4910(9)$ Å, $\beta=116.17°$, and Pearson symbol mC34–1.8 with 32 atoms in the unit cell (8 Co/Ni and 24 Al), which are placed on nine crystallographically inequivalent atomic positions (2 Co/Ni and 7 Al). Two of these are partially occupied [Al(6) by 90% and Al(6′) by 10%]. X-ray diffraction data revealed that the $Al_{13-x}(Co_{1-y}Ni_y)_4$ phase is identical to the previously reported Y phase, found as predominant phase in samples with compositions $Al_{75}Co_{20}Ni_5$ and $Al_{75}Co_{15}Ni_{10}$.[17,24] The structure of $Al_{13-x}(Co_{1-y}Ni_y)_4$ is built up of one type of flat atomic layers, which are related to each other by a 2_1 axis, giving ≈ 0.4 nm period along the [0 1 0] direction (corresponding to the periodic direction in the related *d*-Al-Ni-Co quasicrystal) and two atomic layers within one periodicity unit. Locally, the structure shows close resemblance to the *d*-$Al_{70}Co_{15}Ni_5$ quasicrystal,[25] which also consists of only one type of a quasiperiodic layer, repeated by a 10_5 axis and giving the same ≈ 0.4 nm period.

The single crystal used in our study was grown from an incongruent Al-rich melt of initial composition $Al_{81.9}Co_{14.5}Ni_{3.6}$ by the Czochralski method using a native seed. The composition of the crystal (rounded to the closest integers) was $Al_{76}Co_{22}Ni_2$ and its structure matched well to the monoclinic unit cell of the model of Zhang *et al.*[17] (who studied the composition $Al_{75}Co_{22}Ni_3$). In order to perform crystalline-direction-dependent studies, we have cut from the ingot three bar-shaped samples of dimensions $2\times 2\times 6$ mm^3, with their long axes along three orthogonal directions. The long axis of the first sample was along [0 1 0] direction (designated in the following as *b*), which corresponds to the periodic direction in the related *d*-Al-Ni-Co quasicrystal. The (a,c) monoclinic plane corresponds to the quasiperiodic plane in *d*-QCs and the second sample was cut with its long axis along [0 0 1] (c) direction, whereas the third one was cut along the direction perpendicular to the (b,c) plane. This direction is designated as a^* (it lies in the monoclinic plane at an angle 26° with respect to a and perpendicular to c). For each sample, the orientation of the other two crystalline directions was also known. The so-prepared samples enabled us to determine the anisotropic physical properties along the three orthogonal directions of the investigated monoclinic $Al_{76}Co_{22}Ni_2$, abbreviated as Y-Al-Ni-Co in the following.

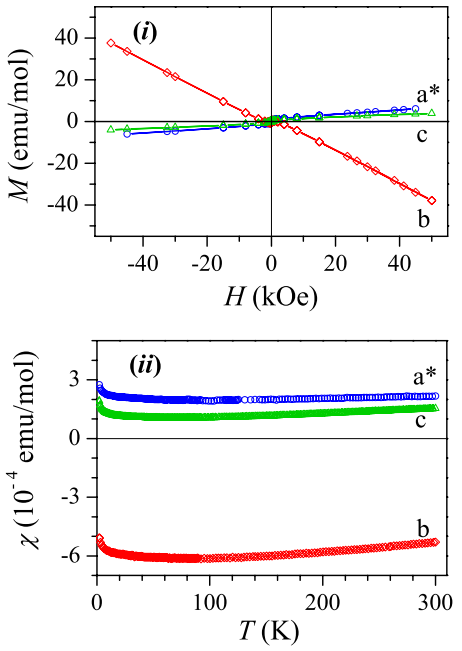

FIG. 1. (Color online) (i) Magnetization M of Y-Al-Ni-Co as a function of the magnetic field H at $T=5$ K with the field oriented along three orthogonal crystalline directions a^*, b, and c. (ii) Temperature-dependent magnetic susceptibility $\chi=M/H$ in the field $H=10$ kOe applied along the three crystalline directions.

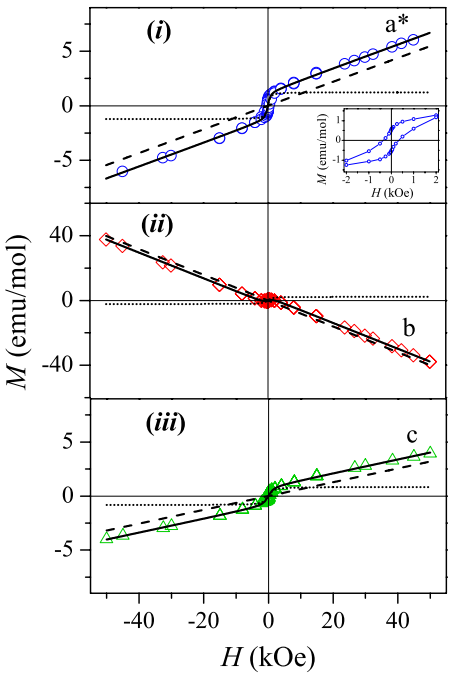

FIG. 2. (Color online) $M(H)$ curves from Fig. 1 on an expanded vertical scale [panel (i): a^* direction, panel (ii): b direction, and panel (iii): c direction]. Solid curves are fits with Eq. (1), dashed lines represent the term of the magnetization linear in the magnetic field kH (the Larmor core contribution and the contribution due to the conduction electrons), and dotted curves are the FM contribution. Fit parameters are given in Table I. The $M(H)$ hysteresis of the FM contribution on an expanded horizontal scale around $H=0$ is shown as an inset in panel (i).

III. ANISOTROPIC PHYSICAL PROPERTIES

A. Magnetization and magnetic susceptibility

The magnetization as a function of the magnetic field, $M(H)$, and the temperature-dependent magnetic susceptibility, $\chi(T)$, were investigated in the temperature interval between 300 and 2 K, using a Quantum Design superconducting quantum interference device (SQUID) magnetometer, equipped with a 50 kOe magnet. In the orientation-dependent measurements, magnetic field was directed along the long axis of each sample, thus along the a^*, b, and c crystalline directions. The $M(H)$ curves at $T=5$ K are displayed in the upper panel of Fig. 1, showing linear dependence of the magnetization on the magnetic field in the whole investigated field range up to 50 kOe, except in the vicinity of $H=0$, where small hysteresis loops are observed for all three directions due to a small ferromagnetic (FM) component in the magnetization. The $M(H)$ curves show astonishing anisotropy: the slopes for the two in-plane directions a^* and c are positive paramagnetic and there is little difference in magnitude between these two directions. In contrast, the $M(H)$ slope for the field along the b direction (periodic direction in d-QC) is much larger and *negative* diamagnetic.

The experimental $M(H)$ curves were reproduced theoretically by the expression

$$M = M_0 L(\mu, H, T) + kH. \quad (1)$$

The first term describes the FM contribution, where M_0 is the saturated magnetization and $L(x)=\coth(x)-1/x$ is the Langevin function that is a limit of the Brillouin function for large spins (or magnetic moments μ). This function reproduces well the $M(H)$ dependence of the FM component, but with an unphysically large μ, so that its validity is merely to enable extraction of the second term, kH, from the total magnetization. Here k represents terms in the susceptibility $\chi=M/H$ that are linear in the magnetic field (the Larmor core diamagnetic susceptibility and the susceptibility of conduction electrons—the Pauli-spin paramagnetic and the Landau orbital diamagnetic contributions). The fits for all three directions with Eq. (1) are shown as solid curves in Fig. 2, where the $M(H)$ curves are displayed on an expanded vertical scale, and the fit parameters are given in Table I. An expanded portion of the M_{a^*} curve on the horizontal scale in the vicinity of $H=0$, showing the hysteresis loop, is shown as an inset in the upper panel of Fig. 2. The loop saturates already in a low field of $H\approx 2$ kOe, a value typical for a FM hysteresis. The microscopic origin of the tiny FM component is not clear, but identical FM contribution was reported also for the related d-$Al_{72}Ni_{12}Co_{16}$ (Ref. 26) and d-$Al_{70}Ni_{15}Co_{15}$ (Ref. 27) quasicrystals, where it was suggested to originate from the Ni and/or Co clusters at the phason boundaries or from small amounts of secondary phases formed mainly by Ni and/or Co. From Table I it is seen that the absolute value of the negative k for the b direction is one order of magnitude larger than the k values for the two in-plane directions a^* and c. The linear $M(H)$ dependence for all three directions up to the highest investigated field suggests predominant role of conduction electrons in the magnetism of Y-Al-Ni-Co.

TABLE I. Parameters of the $M(H)$ fits (solid lines in Fig. 2) using Eq. (1) and $\chi(T)$ fits (solid lines in Fig. 3) using Eq. (2). μ_B stands for the Bohr magneton. The figures in units emu/mol are given per mole of sample (i.e., per mole of the $Al_{76}Co_{22}Ni_2$ compound).

Crystalline direction	M_0 (emu/mol)	μ (μ_B)	k (emu/mol Oe)	χ_0 (emu/mol)	C (emu K/mol)	θ (K)	A_2 (emu/mol K^2)	A_4 (emu/mol K^4)
a^*	1.24	236	1.1×10^{-4}	1.9×10^{-4}	6.3×10^{-4}	−6.2	3.4×10^{-10}	-3.0×10^{-16}
b	2.22	141	-8.0×10^{-4}	-6.3×10^{-4}	9.4×10^{-4}	−6.5	9.9×10^{-10}	1.0×10^{-15}
c	0.84	116	6.4×10^{-5}	1.0×10^{-4}	3.8×10^{-4}	−2.1	7.5×10^{-10}	-1.4×10^{-15}

The temperature-dependent magnetic susceptibility $\chi(T)$ along the three crystalline directions, measured in a field of 10 kOe, is displayed in the lower panel of Fig. 1. The two in-plane susceptibilities χ_{a^*} and χ_c are positive paramagnetic and there is not much difference in their magnitudes. In contrast, the susceptibility in the perpendicular direction χ_b is negative diamagnetic with a much larger absolute value, in agreement with the anisotropic behavior of the $M(H)$ curves shown in the upper panel of Fig. 1. The temperature-dependent susceptibilities are shown on an expanded scale in Fig. 3. For all three crystalline directions, $\chi(T)$'s show a decreasing behavior upon cooling from RT to about 50 K, where a minimum is observed, followed by a $1/T$-type increase upon further cooling toward $T\rightarrow0$. The $\chi(T)$ data were fitted with the expression

$$\chi = \chi_0 + \frac{C}{T-\theta} + A_2T^2 + A_4T^4. \qquad (2)$$

Here χ_0 is a temperature-independent term, $C/(T-\theta)$ is the Curie-Weiss susceptibility of fixed paramagnetic ions, where

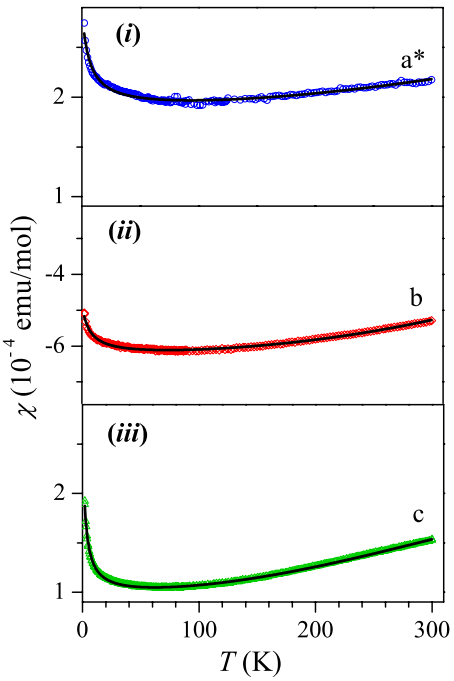

FIG. 3. (Color online) $\chi(T)$ curves from Fig. 1 on an expanded vertical scale [panel (i): a^* direction, panel (ii): b direction, and panel (iii): c direction]. Solid lines are fits with Eq. (2) and fit parameters are given in Table I.

C is the Curie constant and θ the Curie-Weiss temperature, and the terms A_iT^i $(i=2,4)$ are the temperature-dependent corrections that determine the $\chi(T)$ behavior in the high-temperature range above the minimum. The term χ_0 includes the Larmor diamagnetic susceptibility due to closed atomic shells, estimated from literature tables[28] to amount $\chi_{\text{Larmor}}=-4.4\times10^{-4}$ emu/mol, and the FM contribution that is already saturated in the applied field of 10 kOe. The fits with Eq. (2) are shown as solid lines in Fig. 3 and the fit parameters are given in Table I.

The Curie-Weiss paramagnetic susceptibility can be assigned to the paramagnetic Co and Ni atoms in the Y-Al-Ni-Co structure and/or to the extrinsic paramagnetic impurities. In order to see how strong is the Curie-Weiss term as compared to other sources of magnetization, we estimated the fraction of magnetic atoms in the samples from the Curie constant C. To simplify the analysis, we replaced Ni atoms by Co (i.e., we considered the composition $Al_{76}Co_{24}$ instead of the correct one $Al_{76}Co_{22}Ni_2$), which enabled us to determine the fraction of magnetic Co atoms relative to the total number of Co atoms in the sample. Assuming Co^{2+} valence state with the effective Bohr magneton number $p_{\text{eff}}=4.8$, we recalculate C from Table I (given there in units of *per mole of sample*) in units of per mole of Co (i.e., divide by 24, the number of moles of Co in 1 mol of $Al_{76}Co_{24}$). From the obtained value we calculate the mean effective Bohr magneton number $\bar{p}_{\text{eff}}$ (the mean p_{eff} of all the Co atoms in the sample) by using the formula[29] $\bar{p}_{\text{eff}}=2.83\sqrt{C}$. The magnetic Co fraction is then obtained from $f=(\bar{p}_{\text{eff}}/p_{\text{eff}})^2$. For the three investigated crystalline directions we obtained $f_{a^*}=9\times10^{-6}$, $f_b=14\times10^{-6}$, and $f_c=5\times10^{-6}$ (yielding $\bar{f}\approx9\pm5$ ppm, when averaged over the three directions), revealing that only a few ppm of Co atoms carry magnetic moments, the rest being nonmagnetic. As the concentration of external magnetic impurities is also of the order of ppm, external impurities may contribute significantly to the observed Curie-Weiss magnetization as well. Due to the smallness of these figures, Y-Al-Ni-Co can be considered as a nonmagnetic alloy with the usual "contamination" by paramagnetic impurities, leading to the Curie upturn in the susceptibility at low temperatures. The nonmagnetic nature of Y-Al-Ni-Co is similar to that of the d-Al-Ni-Co quasicrystal, where its nonmagnetic character was demonstrated by the observation of intense ^{59}Co line at the Larmor frequency in the NMR spectrum of single-crystalline d-$Al_{72.6}Co_{16.9}Ni_{10.5}$,[30] i.e., the ^{59}Co NMR line did not exhibit any paramagnetic shift, typical of paramagnetic solids. As the magnetic Co fraction in Y-Al-Ni-Co is very small, the negative Curie-Weiss temperatures in Table I should be considered as additional fit parameters only,

which slightly improve the fits and not as an indication of an antiferromagnetic (AFM) coupling between the diluted paramagnetic ions.

Due to the negligible role of Curie paramagnetism in Y-Al-Ni-Co, the temperature corrections A_2T^2 and A_4T^4 are straightforward to associate with the temperature-dependent susceptibility of conduction electrons. One possibility is to assume a temperature-dependent Pauli-spin susceptibility. Within the independent-electron approximation, the spin part of the electronic magnetization can be written as

$$\chi_{\text{Pauli}} = \chi_P^0 + A_2T^2 + A_4T^4. \quad (3)$$

Here $\chi_P^0 = \mu_B^2 g(E_F)$ is the temperature-independent term [where μ_B is the Bohr magneton and $g(E_F)$ is the DOS at E_F] and A_2T^2 and A_4T^4 are the two lowest-order temperature corrections, emerging from the temperature dependence of the chemical potential and the variation of the DOS with energy in the vicinity of E_F. Assuming that the DOS around E_F can be expanded in Taylor series, we have $A_2 = \chi_P^0(\pi^2 k_B^2/6)\{(g''/g) - (g'/g)^2\}$, where $g = g(E_F)$, $g' = (\partial g/\partial E)_{E_F}$, and $g'' = (\partial^2 g/\partial E^2)_{E_F}$. The explicit form of A_4 can be found, e.g., in Ref. 31 and depends on the DOS derivatives at E_F up to the fourth order. In order that the expansion of Eq. (3) is meaningful, the temperature correction terms must converge, i.e., the lower-order term A_2T^2 must be larger than the higher one A_4T^4. The fit-determined A_2 and A_4 values from Table I reveal that this is the case. At $T = 200$ K, we get the ratios $A_2T^2/|A_4T^4| = 28$, 25, and 14 for the a^*, b, and c directions, respectively, whereas at 300 K, these ratios become 13, 11, and 6. The convergence of the T-dependent corrections is reasonable, so that the assumption of a temperature-dependent Pauli-spin susceptibility remains a valid possibility to explain the increasing conduction-electron susceptibility upon heating.

The second possible explanation is the temperature-dependent Landau diamagnetic contribution due to orbital circulation of the conduction electrons. For a free-electron metal, χ_{Landau} is temperature independent and related to χ_{Pauli} by a fixed ratio. Abandoning the free-electron picture, it is plausible to assume that a decreasing electron mean-free path between scattering events will also diminish the electron orbital motion in a magnetic field and consequently reduce (in absolute value) the negative Landau diamagnetic susceptibility. It will be shown in the following that the electrical resistivity $\rho(T)$ of Y-Al-Ni-Co exhibits PTC in the whole investigated temperature range from 2 to 300 K at metallic values (10–80 $\mu\Omega$ cm) for all three crystalline directions, demonstrating that the electron-phonon scattering is the main mechanism of the resistivity increase upon heating. In such low-resistivity metallic alloys, the increase in $\rho(T)$ is entirely due to shortening of the electron mean-free path. This shortening will also diminish the electronic circular motion and consequently decrease the absolute value of the diamagnetic (negative) χ_{Landau}, so that the sum $\chi = \chi_{\text{Pauli}} + \chi_{\text{Landau}}$ will be an increasing function of temperature in very much the same manner as the resistivity $\rho(T)$ itself. A comparison of the $\chi(T)$ curves from Fig. 3 (neglecting the Curie upturns at low temperatures) to the $\rho(T)$ curves from Fig. 4 shows that these two quantities exhibit qualitatively similar temperature behavior. Considering the temperature-dependent Landau diamagnetism to be at the origin of the temperature-dependent conduction-electron magnetism in Y-Al-Ni-Co, the terms A_2T^2 and A_4T^4 in Eq. (2) should not be considered as the two lowest-order temperature corrections to the Pauli susceptibility, but the entire Eq. (2) (excluding the Curie-Weiss term) should be considered merely as a polynomial fit to the susceptibility, where the weak temperature increase in χ upon heating results from the mean-free-path shortening effect on the Landau diamagnetic susceptibility.

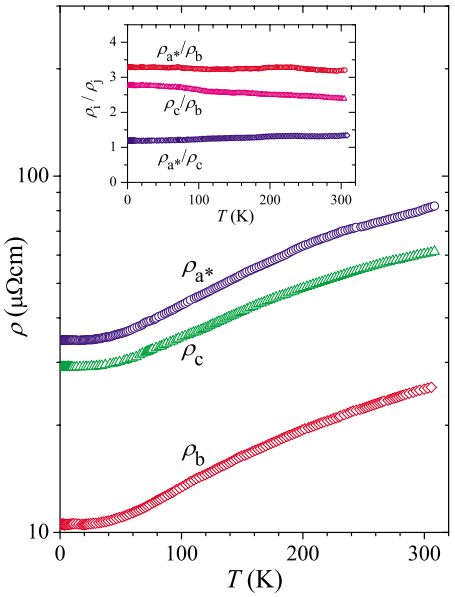

FIG. 4. (Color online) Temperature-dependent electrical resistivity of Y-Al-Ni-Co along three orthogonal crystalline directions a^*, b, and c (note that the vertical scale is logarithmic). The inset shows the resistivity ratios ρ_i/ρ_j $(i,j = a^*, b, c)$.

Identical temperature-dependent $\chi(T)$'s to those of Y-Al-Ni-Co from Fig. 3 were also found in the related complex intermetallics β-Al_3Mg_2 (Ref. 32) and the "Bergman" phase[33] $Mg_{32}(Al,Zn)_{49}$, which both show similar PTC electrical resistivities with low values in the range 30–50 $\mu\Omega$ cm. For these two compounds, the question whether the weak temperature dependence of the conduction-electron susceptibility originates from the temperature corrections to the Pauli-spin susceptibility or from the temperature-dependent Landau susceptibility was solved by determining experimentally the sole Pauli susceptibility from the Knight shift of the[27] Al NMR line,[32,33] owing to the fact that the Knight shift is linearly proportional to χ_{Pauli}. The results have shown that χ_{Pauli} is independent of the temperature, so that the temperature dependence of χ could be unambiguously associated with the temperature-dependent Landau susceptibility. Due to the very similar magnitudes and temperature dependencies of $\chi(T)$ and $\rho(T)$ of Y-Al-Ni-Co, β-Al_3Mg_2, and $Mg_{32}(Al,Zn)_{49}$, the origin of the temperature-dependent conduction-electron susceptibility in Y-Al-Ni-Co is very likely the same as in the other two compounds (the Landau term), though an additional contribution due to the temperature-dependent corrections to the Pauli-spin susceptibility cannot be excluded on the basis of the above analysis.

The main result of the magnetic measurements of Y-Al-Ni-Co is the strong anisotropy of the conduction-electron susceptibility along the three crystalline directions. While this susceptibility is paramagnetic for the field directed along the two in-plane directions a^* and c, it is diamagnetic for the perpendicular b direction. The origin of this anisotropy should have its microscopic origin in the anisotropy of the Fermi surface, as a consequence of the structural anisotropy of Y-Al-Ni-Co along different crystalline directions. This anisotropy will be discussed further together with the anisotropy of the electrical resistivity in terms of the crystalline-direction-dependent local atomic order on the scale of near-neighbor atoms, pertinent to the specific structure of the Y-Al-Ni-Co phase.

Comparing magnetic anisotropy of the Y-Al-Ni-Co decagonal approximant to the anisotropy of the *d*-Al-Ni-Co quasicrystal, the following analogy is observed. Magnetic susceptibility of *d*-$Al_{72}Ni_{12}Co_{16}$ also exhibits anisotropy[26] for the magnetic field directed either along the periodic direction or lying within the quasiperiodic plane. For both orientations, the $M(H)$ curves also show small FM component around $H=0$. While for the Y-Al-Ni-Co, the $M(H)$ relation is negative diamagnetic for the field along the b direction (corresponding to the periodic direction in *d*-Al-Ni-Co) and positive paramagnetic for the two in-plane directions a^* and c, the $M(H)$ relation of *d*-Al-Ni-Co is negative diamagnetic for the field along both the periodic direction and the quasiperiodic plane. The diamagnetic slopes are, however, different for the two directions, being larger for the periodic direction. The stronger diamagnetism of *d*-Al-Ni-Co along the periodic direction is thus in good analogy to the diamagnetism of Y-Al-Ni-Co along b, whereas the weaker in-plane diamagnetism of *d*-Al-Ni-Co is changed into a weak in-plane paramagnetism in Y-Al-Ni-Co.

B. Electrical resistivity

Electrical resistivity was measured between 300 and 2 K using the standard four-terminal technique. To eliminate the effect of the contact potential, the dc current direction was reversed between $\pm j$ and the data points were measured and averaged for the two current directions. The $\rho(T)$ data for the three crystalline directions are displayed in Fig. 4. The resistivity is the lowest along the b direction perpendicular to the atomic planes, where its RT value amounts $\rho_b^{300\ \mathrm{K}}=25\ \mu\Omega$ cm and the residual resistivity is $\rho_b^{2\ \mathrm{K}}=10\ \mu\Omega$ cm. The two in-plane resistivities are higher, amounting $\rho_c^{300\ \mathrm{K}}=60\ \mu\Omega$ cm and $\rho_c^{2\ \mathrm{K}}=29\ \mu\Omega$ cm for the c direction and $\rho_{a^*}^{300\ \mathrm{K}}=81\ \mu\Omega$ cm and $\rho_{a^*}^{2\ \mathrm{K}}=34\ \mu\Omega$ cm for the a^* direction. While ρ_b is considerably smaller than ρ_{a^*} and ρ_c by a factor of about 3, the two in-plane resistivities are much closer, $\rho_{a^*}/\rho_c \approx 1.3$. The above resistivity values, appearing in the order $\rho_{a^*} > \rho_c \gg \rho_b$, reveal that Y-Al-Ni-Co is good electrical conductor along all three crystalline directions. It is interesting to note that the ratios of the resistivities along different crystalline directions vary little over the whole investigated temperature range 300–2 K (inset of Fig. 4), amounting at RT $\rho_{a^*}/\rho_b \approx 3.2$, $\rho_c/\rho_b \approx 2.5$, and $\rho_{a^*}/\rho_c \approx 1.3$. This demonstrates that $\rho(T)$'s along the three crystalline directions exhibit the same type of PTC temperature dependence. The strong PTC of the resistivity along all three crystalline directions demonstrates predominant role of the electron-phonon-scattering mechanism.

Comparing the anisotropic resistivity of Y-Al-Ni-Co to that of the *d*-Al-Ni-Co quasicrystal,[2] we find that the resistivities of both compounds are about the same along the "periodic" direction (b in the case of Y-Al-Ni-Co) in both magnitude ($10-40\ \mu\Omega$ cm) and PTC temperature dependence. The in-plane resistivities are in both cases larger, but there exists significant difference between the two compounds. While the two in-plane resistivities ρ_{a^*} and ρ_c of Y-Al-Ni-Co show the same metallic PTC dependence as ρ_b, but are increased by factors about 3.2 and 2.5, respectively, the in-plane resistivity of *d*-Al-Ni-Co is qualitatively different, showing nonmetallic NTC, and about ten times larger value at RT than the resistivity along the periodic direction. While from the anisotropic-resistivity point of view *d*-Al-Ni-Co quasicrystal can be considered exceptional, its decagonal approximant Y-Al-Ni-Co is not special and behaves as a regular conductor.

In an anisotropic crystal, the electrical conductivity $\boldsymbol{\sigma}$ (the inverse resistivity $\boldsymbol{\rho}^{-1}$) is generally a symmetric (and diagonalizable) tensor, relating the current density $\vec{j}$ to the electric field $\vec{E}$ via the relation $j_i=\Sigma_j \sigma_{ij} E_j$, where $i,j=x,y,z$ denote crystalline directions. Using the linearized Boltzmann transport equation, the conductivity-tensor elements σ_{ij} are given by[34]

$$\sigma_{ij} = \frac{e^2}{4\pi^3\hbar} \int \frac{\tau v_i v_j dS_F}{v_{k_\perp}}, \tag{4}$$

where τ is the relaxation time, v_i are the components of the electron velocity, $v_{k_\perp}$ is the component of velocity perpendicular to the Fermi surface, and $\int dS_F$ represents surface integral in the k space over the Fermi (constant energy) surface.

The geometry of our samples (their long axes were along three orthogonal directions a^*, b, and c) and the direction of the electric field applied along their long axes imply that diagonal elements $\sigma_{xx}=\sigma_{a^*}$, $\sigma_{yy}=\sigma_b$, and $\sigma_{zz}=\sigma_c$ were measured in our experiments in a Cartesian x,y,z coordinate system. Due to the monoclinic symmetry of the unit cell of Y-Al-Ni-Co, the conductivity tensor is not diagonal in this system.

In order to perform quantitative theoretical analysis of the anisotropic resistivity of Y-Al-Ni-Co, evaluation of the tensor elements σ_{ij} given by Eq. (4) requires knowledge of the anisotropic Fermi surface. It is the assumption of a spherical Fermi surface, applied to Eq. (4), that leads to the known expressions of electrical conduction in metals as given by the theories of Ziman, Baym, Bloch-Grüneisen, and Baym-Meisel-Cote,[35] so that these theories are valid for isotropic solids. For anisotropic solids, the analysis should start from Eq. (4) using the compound-specific anisotropic Fermi surface. In the following we perform *ab initio* calculation of the Fermi surface for the Y-Al-Ni-Co and estimate the resistivity ratios ρ_i/ρ_j along the investigated crystalline directions.

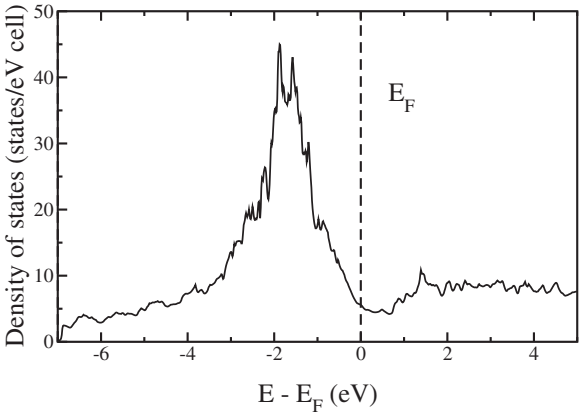

FIG. 5. Theoretical electronic DOS of the Y-Al-Ni-Co phase, calculated *ab initio* for the structural model of Zhang *et al.* (Ref. 17). Ni atoms have been replaced by Co, so that the calculation was performed for the composition $Al_{75}Co_{25}$ instead of the Zhang composition $Al_{75}Co_{22}Ni_3$.

C. Fermi surface and the density of states

The *ab initio* calculation of the electronic structure was performed within the framework of the density-functional theory by applying WIEN97 code,[36] which adopts the full-potential linearized-augmented-plane-wave (FLAPW) method.[37] Calculations were based on the Y-Al-Ni-Co structural model by Zhang *et al.*,[17] where we have replaced Ni atoms by Co (thus considering the composition $Al_{75}Co_{25}$ instead of the "Zhang" composition $Al_{75}Co_{22}Ni_3$). The partially occupied sites Al(6) and Al(6′) were taken with probabilities 1 and 0, respectively. The muffin-tin radii around the atoms were 1.16 Å that yielded the basis-set energy cutoff parameter of 10 eV. The k-space summation was performed using 180 k points in the full Brillouin zone (BZ) in terms of the modified tetrahedron method.[38] The criterion for the self-consistency was the difference in the total energy after the last two iterations, being less than 1×10^{-4} Ry. The calculated electronic DOS is presented in Fig. 5. It is strongly dominated by the transition-metal $3d$ states and exhibits a modest pseudogap close to the Fermi level without any spikes. The calculated Fermi surface in the first BZ is displayed in Fig. 6 using the drawing program XCRYSDEN.[39] It is contributed by 11 bands that cross E_F, resulting in a significant complexity. The Fermi surface is highly anisotropic, providing the origin of the experimentally observed anisotropy in the electrical conductivity.

The ratios of the anisotropic conductivities along the investigated crystalline directions were estimated starting from Eq. (4) and using the Fermi surface displayed in Fig. 6. The relaxation time τ was considered energy independent in the vicinity of E_F and was taken out of the integral. For the Fermi surface consisting of 11 branches, the conductivity-tensor diagonal elements were rewritten in the form

$$\sigma_{ii} = \sum_{n=1}^{11} \int_{E_n(\vec{k})=E_F} \frac{dS_F^n}{|\nabla_{k_\perp} E_n(\vec{k})|} \left(\frac{\partial E_n(\vec{k})}{\partial k_i} \right)^2, \quad i = x,y,z, \quad (5)$$

where all constant factors were set to unity and n is the index of a band with the energy dispersion relation $E_n(\vec{k})$. In deriving Eq. (5), the relation $\vec{v}_n(\vec{k}) = (1/\hbar)\nabla_{\vec{k}} E_n(\vec{k})$ for the mean velocity of an electron in a level with band index n and wave vector $\vec{k}$ was used, whereas $v_{n\perp} = (1/\hbar)\nabla_{k_\perp} E_n(\vec{k})$ is the velocity component perpendicular to the Fermi surface. Equation (5) gives the conductivities at zero temperature, $\sigma(T=0)$.

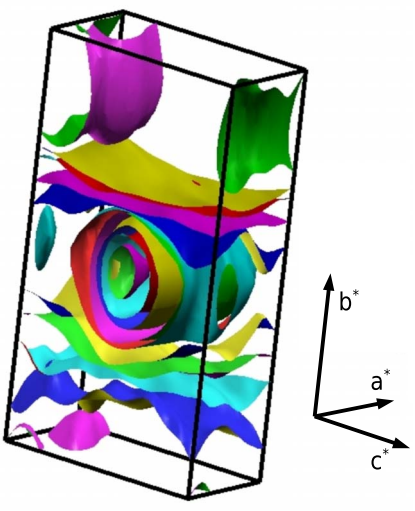

FIG. 6. (Color online) Fermi surface of Y-Al-Ni-Co in the first Brillouin zone, calculated *ab initio* for the structural model of Zhang *et al.* (Ref. 17) (considering the composition $Al_{75}Co_{25}$ instead of the Zhang composition $Al_{75}Co_{22}Ni_3$). Orientation of the reciprocal space axes a^*, b^*, and c^* is also shown. While a^* and c^* are perpendicular to b^*, the angle between a^* and c^* amounts 63.83°.

Numerical integration of Eq. (5) was performed along the lines of Ref. 40. The convergence with respect to the number of applied k points was very demanding. However, it was found that 510 k points from the full BZ were enough to obtain reasonably well-converged conductivity ratios. Considering resistivities instead of the conductivities, the theoretical resistivity ratios were found to amount $\rho_{a^*}/\rho_c = 1.1$, $\rho_c/\rho_b = 1.7$, and $\rho_{a^*}/\rho_b = 1.9$, to be contrasted with the experimental $T\to0$ ratios (see inset of Fig. 4) 1.2, 2.8, and 3.3, respectively. The theory thus gives the resistivities in the order $\rho_{a^*} > \rho_c > \rho_b$, which is the same as observed experimentally (Fig. 4). Good quantitative agreement is obtained for the ρ_{a^*}/ρ_c ratio (theoretical 1.1 value versus the experimental 1.2), whereas for the other two ratios, the agreement is qualitative. One reason for this discrepancy is the fact that experimental resistivities upon $T\to0$ are limited by extrinsic effects—impurities and defects—whereas theoretical calculations assume a perfect lattice. In view of that, the agreement of the above theoretical and experimental resistivity ratios can be considered as satisfactory.

D. Thermoelectric power

The thermoelectric power (the Seebeck coefficient S) was measured between 300 and 2 K by using a standard temperature-gradient technique. The sample was mounted on two small, electrically insulated copper thermal reservoirs. Electrical connections to the sample were made via annealed

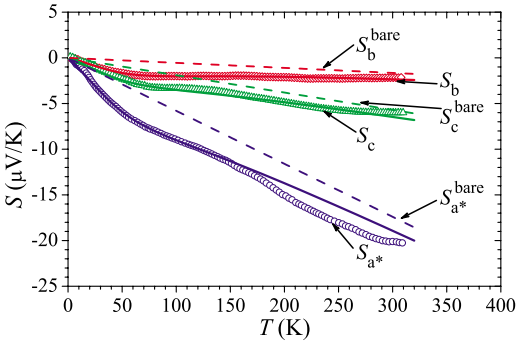

FIG. 7. (Color online) Temperature-dependent thermoelectric power (the Seebeck coefficient S) of Y-Al-Ni-Co along three orthogonal crystalline directions a^*, b, and c. Solid curves are fits with Eqs. (6) and (8) and the fit parameters are given in Table II. Bare thermopowers (in the absence of electron-phonon interactions) are shown by dashed lines.

gold leads attached to its ends using silver paint. The temperature difference on the sample was measured by means of a differential Au(0.03% Fe)-Chromel thermocouple with junctions glued by a General Electric varnish as close as possible to the electrical connections for measuring the thermopower. At each temperature, we have reversed the temperature difference on the sample several times, keeping it lower than 1 K. The experimental setup was checked by measuring a piece of a lead wire. The anisotropic thermopower data of Y-Al-Ni-Co are displayed in Fig. 7. Thermopower is negative for all three directions, suggesting that electron-type carriers dominate the thermoelectric transport. The RT values are in the range between −2 and −20 μV/K in the order $|S_{a^*}|>|S_c|>|S_b|$. The $S(T)$ characteristics for all directions are qualitatively similar, except for the variation in magnitude. In all cases, a change in slope is observed at about 70 K, where the low-temperature slope is higher than the high-temperature one. Nonlinearities in the thermopower in this temperature range are often associated with electron-phonon effects, which typically reach their maximum value at a temperature that is some fraction of the Debye temperature θ_D. The thermopower in all three directions extrapolates approximately linearly to zero upon $T\rightarrow 0$, a feature that is usually associated with metallic diffusion thermopower. These features allow comparing the $S(T)$ data from Fig. 7 to the behavior expected for the electron-phonon enhancement of diffusion thermopower, as observed in several metallic glasses[41] and also in the related d-$Al_{73}Co_{10}Ni_{17}$ quasicrystal.[42] The importance of phonons in the temperature dependence of the thermopower of Y-Al-Ni-Co is analogous to the temperature-dependent electrical resistivity of this compound, where electron-phonon interaction represents the main scattering mechanism, leading to the PTC of the resistivity.

The electron-phonon enhancement of the diffusion thermopower can be written as[41,42]

$$\frac{S}{T}=\frac{S^{\text{bare}}}{T}[1+\lambda(T)], \tag{6}$$

where S^{bare} is the bare thermopower in the absence of the electron-phonon interaction and $\lambda(T)$ is the electron-phonon mass enhancement parameter given by[41]

TABLE II. Fit parameters of the anisotropic thermopower using Eqs. (6) and (8).

Crystalline direction	S^{bare}/T (μV/K^2)	$\lambda(0)$
a^*	-5.8×10^{-2}	1.0
b	-5.5×10^{-3}	5.0
c	-1.9×10^{-2}	1.6

$$\lambda(T)=\int_0^\infty d\omega\frac{\alpha^2F(\omega)}{\omega}G\left(\frac{\hbar\omega}{k_BT}\right). \tag{7}$$

Here $\alpha^2F(\omega)$ is the Eliashberg function and $G(\hbar\omega/k_BT)$ is a universal function, introduced by Kaiser.[41] Full treatment of the anisotropic thermopower should take into account the anisotropy of $\alpha^2F(\omega)$, which is beyond our possibilities. To simplify the problem, we adopt the same approximation as applied before to the d-Al-Ni-Co quasicrystal[42] using the Debye model, $\alpha^2F(\omega)=C_D\omega^n$, with a cutoff frequency $\omega_D=k_B\theta_D/\hbar$, where the anisotropy is introduced phenomenologically through the orientation-dependent parameters C_D and n. Equation (7) then becomes

$$\lambda(T)=C_D\int_0^{\omega_D}d\omega\omega^{n-1}G\left(\frac{\hbar\omega}{k_BT}\right). \tag{8}$$

Our fits of the anisotropic thermopower (solid curves in Fig. 7) could be satisfactorily made with $n=2$, so that only C_D was varied for different crystalline directions. We observe that Eqs. (6) and (8) reproduce well the change in slope in the thermopowers at about 70 K. While the fits for the b and c directions are satisfactory up to RT, the fit for the a^* direction is good up to 150 K, whereas it starts to deviate from the measured data at higher temperatures. At present we do not have an explanation for this deviation. The fit parameters are given in Table II, where the value $\lambda(0)=C_D\omega_D^2/2$ is given instead of C_D [taking into account that $\lim_{T\rightarrow0}G(\hbar\omega/k_BT)=1$ in Eq. (8)]. The Debye temperature was taken as $\theta_D=320$ K. The bare thermopowers S^{bare} for all three crystalline directions are shown as dashed lines in Fig. 7.

The anisotropy of the so-extracted bare thermopowers can now be analyzed using the well-known expression derived from the linearized Boltzmann transport equation,

$$S^{\text{bare}}=\frac{\pi^2}{3(-e)}k_B^2T\left[\frac{\partial\ln\sigma(E)}{\partial E}\right]_{E=\zeta}, \tag{9}$$

where ζ is the chemical potential and $\sigma(E)$ is the spectral conductivity in the vicinity of the Fermi level. Since $\sigma(E)$ is not known, we made the following qualitative analysis. The geometry of our samples requested that we have experimentally measured the diagonal elements of the thermopower tensor in the Cartesian coordinate system,

$$S_{ii}^{\text{bare}}=\frac{\pi^2}{3(-e)}k_B^2T\rho_{ii}\left[\frac{\partial\sigma_{ii}(E)}{\partial E}\right]_{E=\zeta}. \tag{10}$$

The smoothly varying DOS in the vicinity of E_F from Fig. 5 suggests that there are no sharp features in $\sigma(E)$ close to the

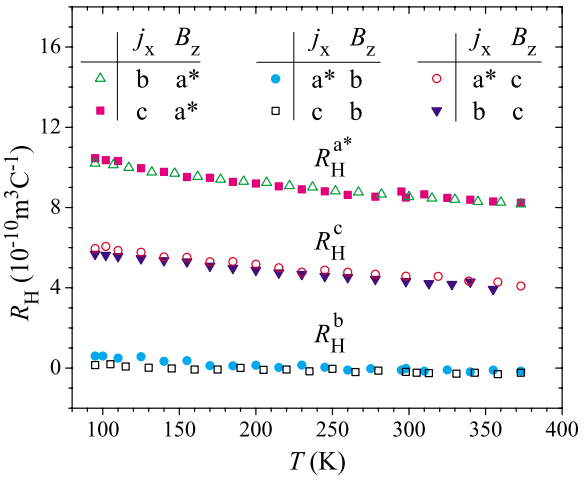

FIG. 8. (Color online) Anisotropic temperature-dependent Hall coefficient $R_H=E_y/j_xB_z$ of Y-Al-Ni-Co for different combinations of directions of the current j_x and magnetic field B_z (given in the legend). The superscript a^*, b, or c on R_H denotes the direction of the magnetic field.

Fermi level, so that no singularities in its derivative are expected. Within the approximation that the derivative $[\partial\sigma_{ii}(E)/\partial E]_{E=\zeta}$ does not depend significantly on the crystalline direction, the magnitude of the thermopower in the direction i is predominantly determined by the magnitude of the resistivity ρ_{ii} in that direction. Since $\rho_{a^*}>\rho_c>\rho_b$ (Fig. 4), this requires bare thermopowers in the order $|S^{\text{bare}}_{a^*}/T|>|S^{\text{bare}}_c/T|>|S^{\text{bare}}_b/T|$. Figure 7 and Table II show that this was indeed observed experimentally.

E. Hall coefficient

The Hall-effect measurements were performed by the five-point method using standard ac technique in magnetic fields up to 10 kOe. The current through the samples was in the range 10–50 mA. The measurements were performed in the temperature interval from 90 to 370 K. The temperature-dependent Hall coefficient $R_H=E_y/j_xB_z$ is displayed in Fig. 8. In order to determine the anisotropy of R_H, three sets of experiments were performed with the current along the long axis of each sample (thus along a^*, b, and c), whereas the magnetic field was directed along each of the other two orthogonal crystalline directions, making six experiments altogether. For all combinations of directions, the R_H values are typically metallic in the range 10^{-10} m^3 C^{-1} (with the experimental uncertainty of $\pm 0.1\times10^{-10}$ m^3 C^{-1}), showing weak temperature dependence. This temperature dependence shows tendency to disappear at higher temperatures. R_H's exhibit pronounced anisotropy with the following regularity. The six R_H sets of data form three groups of two practically identical R_H curves, where the magnetic field in a given crystalline direction yields the same R_H for the current along the other two crystalline directions in the perpendicular plane. Thus, identical Hall coefficients are obtained for combinations $R_H^{a^*}=E_b/j_cB_{a^*}$ and $R_H^{a^*}=E_c/j_bB_{a^*}$ (where additional superscript on the Hall coefficient denotes the direction of the magnetic field), amounting $R_H^{a^*}(300\ \text{K})=8.5\times10^{-10}$ m^3 C^{-1}, $R_H^b=E_{a^*}/j_cB_b$ and $R_H^b=E_c/j_{a^*}B_b$ with $R_H^b(300\ \text{K})\approx0$, and $R_H^c=E_b/j_{a^*}B_c$ and $R_H^c=E_{a^*}/j_bB_c$ with $R_H^c(300\ \text{K})\approx4.5\times10^{-10}$ m^3 C^{-1}. The anisotropic R_H values are also collected in Table III.

TABLE III. Anisotropic Hall coefficient $R_H=E_y/j_xB_z$ of Y-Al-Ni-Co for various directions of the current and field.

Current direction (j_x)	Field direction (B_z)	R_H(300 K) (10^{-10} m^3 C^{-1})
a^*	b	0.0
	c	4.6
b	a^*	8.5
	c	4.3
c	a^*	8.5
	b	−0.2

The two rather high positive values $R_H^{a^*}$ and R_H^c for the field lying in the (a,c) atomic plane and the almost zero value of R_H^b for the field along the perpendicular b direction (periodic direction in d-QCs) reflect strong anisotropy of the Fermi surface that consists mostly of holelike parts, whereas electronlike and holelike parts are of comparable importance for the field perpendicular to the (a,c) plane. At the same time, negative thermopower suggests that the Fermi surface is mostly electronlike. While this apparent contradiction can be resolved by considering direction-dependent details of the anisotropic Fermi surface, opposite signs $S<0$ and $R_H>0$ are not uncommon in literature. This situation was discussed for the high-T_c cuprates,[43] where the electrons form an unusual state in which the Hall (cyclotron) mass parallel to the Fermi surface is holelike (<0) but the transport mass perpendicular to it is electronlike (>0). This electronlike transport mass contributes to negative S, while the holelike Hall mass results in positive R_H. In such a state, the electron on the Fermi surface has complete duality; it is holelike in one direction, but electronlike in another. The applicability of this hypothesis to Y-Al-Ni-Co remains to be established. The direction-dependent analysis of the 11-branch Fermi surface of Fig. 6 was not a straightforward task and was not performed here.

Comparing the R_H anisotropy of Y-Al-Ni-Co to the d-QCs, we find qualitative similarity. For d-QCs, universality of the Hall-effect anisotropy was reported for the d-Al-Ni-Co, d-Al-Cu-Co, and d-Al-Si-Cu-Co,[6] where $R_H>0$ for the field lying in the quasiperiodic plane (corresponding to the in-plane coefficients $R_H^{a^*},R_H^c>0$ of Y-Al-Ni-Co), whereas R_H changes sign to negative for the field along the periodic direction (corresponding to $R_H^b\approx0$ of Y-Al-Ni-Co). The above d-QCs also exhibit similar weak temperature dependence of R_H as Y-Al-Ni-Co, so that there is complete analogy between d-QCs and their approximant Y-Al-Ni-Co.

F. Thermal conductivity

Thermal conductivity κ of Y-Al-Ni-Co was measured along the a^*, b, and c directions using an absolute steady-state heat-flow method. The thermal flux through the samples

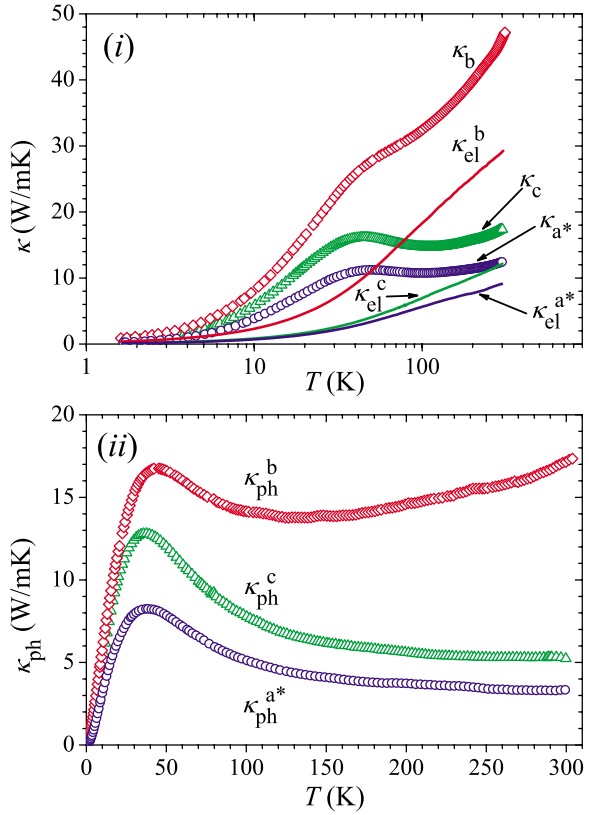

FIG. 9. (Color online) (i) Thermal conductivity κ of Y-Al-Ni-Co along the three crystalline directions a^*, b, and c. Electronic contributions κ_{el}, estimated from the Wiedemann-Franz law, are shown by solid curves. Note the logarithmic temperature scale. (ii) Phononic thermal conductivity $\kappa_{ph}=\kappa-\kappa_{el}$ along the three crystalline directions.

was generated by a 1 kΩ RuO_2 chip resistor, glued to one end of the sample, while the other end was attached to a copper heat sink. The temperature gradient across the sample was monitored by a Chromel-Constantan differential thermocouple. The phononic contribution $\kappa_{ph}=\kappa-\kappa_{el}$ was estimated by subtracting the electronic contribution κ_{el} from the total conductivity using the Wiedemann-Franz law $\kappa_{el}=\pi^2k_B^2T\sigma(T)/3e^2$ and the measured electrical conductivity data $\sigma(T)=\rho^{-1}(T)$ from Fig. 4. Though the use of the Wiedemann-Franz law is a rough approximation, in this way determined κ_{ph} gives an indication of the anisotropy of the phononic spectrum. The total thermal conductivity κ along the three crystalline directions is displayed in the upper panel of Fig. 9 and the electronic contribution κ_{el} is shown by solid curves. At 300 K, we get the following anisotropy: $\kappa^{a^*}=12.5$ W/mK, $\kappa_{el}^{a^*}=9.1$ W/mK with their ratio $(\kappa_{el}^{a^*}/\kappa^{a^*})_{300\ K}=0.73$, $\kappa^b=46.3$ W/mK, $\kappa_{el}^b=29.2$ W/mK with $(\kappa_{el}^b/\kappa^b)_{300\ K}=0.63$, and $\kappa^c=17.4$ W/mK, $\kappa_{el}^c=12.2$ W/mK with $(\kappa_{el}^c/\kappa^c)_{300\ K}=0.70$. Electrons are thus majority heat carriers at RT for all three directions. The anisotropic thermal conductivities appear in the order $\kappa^b>\kappa^c>\kappa^{a^*}$ and similarly $\kappa_{el}^b>\kappa_{el}^c>\kappa_{el}^{a^*}$, which is identical to the order in which the anisotropic electrical conductivities appear (Fig. 4): $\sigma_b>\sigma_c>\sigma_{a^*}$. The phononic thermal conductivity is shown in the lower panel of Fig. 9. We observe that anisotropic κ_{ph}'s again appear in the same order, $\kappa_{ph}^b>\kappa_{ph}^c>\kappa_{ph}^{a^*}$, so that the phononic conductivity is the highest along the b direction perpendicular to the (a,c) atomic layers, whereas the two in-plane conductivities are lower and show smaller anisotropy. For all directions, κ_{ph}'s show a typical phonon umklapp maximum at about 40 K.

While it is expected that the anisotropic electronic thermal conductivities κ_{el} should appear in the same order as the anisotropic electrical conductivities (both are related to the electronic DOS), it is not *a priori* obvious that the anisotropic phononic thermal conductivities should also appear in this order, as κ_{ph} is related to the *vibrational* DOS. Our results nevertheless show that Y-Al-Ni-Co is the best conductor, both electrical and thermal, along the b direction, whereas both conductivities are smaller in the (a,c) plane. In the absence of the anisotropic phonon-dispersion-relation $\omega(\vec{k})$ information for the Y-Al-Ni-Co structure, further analysis of the temperature-dependent anisotropic $\kappa(T)$'s is skipped.

IV. ANISOTROPY VERSUS COMPLEX ATOMIC ORDER

The anisotropy of the above-presented physical parameters (magnetic susceptibility, electrical resistivity, thermoelectric power, Hall coefficient, and thermal conductivity) of Y-Al-Ni-Co arises from the anisotropy of its electronic structure and phononic spectrum. These quantities depend crucially on the anisotropy of the atomic structure, i.e., on the microscopic structural details of the $Al_{13}TM_4$ phase along different crystalline directions. Here we consider possible reasons for the anisotropy of the electrical resistivity and magnetic susceptibility by analyzing structural details of the Y-Al-Ni-Co model by Zhang *et al.*[17]

We consider first the anisotropy of the electrical resistivity. We adopt previous result based on *ab initio* calculations of the electronic charge density in the unit cell of the Al_4TM decagonal approximant[12] suggesting that, in a long-range transport, conduction electrons will preferentially move along aluminum-rich atomic chains along a given crystalline direction. The charge density along Al-only chains is more uniform and hence electron-gas-like (see Fig. 8 of Ref. 12), which makes the motion of electrons along such paths easy, whereas the charge is strongly peaked at the TM atoms, which act as strong scattering centers and increase the resistivity. In order to explain the anisotropic electrical resistivity of Y-Al-Ni-Co, we analyze the structure of the $Al_{13}TM_4$ monoclinic unit cell of the Zhang model by searching for connected Al-only atomic chains along different crystalline directions.

Considering the $Al_{13}TM_4$ structure along the b direction and adopting the nomenclature of Zhang *et al.*,[17] we find two types of Al-only chains propagating along this direction [panel (i) of Fig. 10]. The first are the chains connecting Al(3) atoms only with the Al(3)-Al(3) distance $d_{Al\text{-}Al}=2.59$ Å. In these zigzag atomic chains, the angle between the vector joining two nearest-neighbor Al(3) atoms and the b axis amounts $\theta\approx 38°$. The second chain is formed of Al(5) atoms only with a slightly larger Al(5)-Al(5) distance $d_{Al\text{-}Al}=2.67$ Å and angle $\theta\approx 40°$. Considering next the Al-only

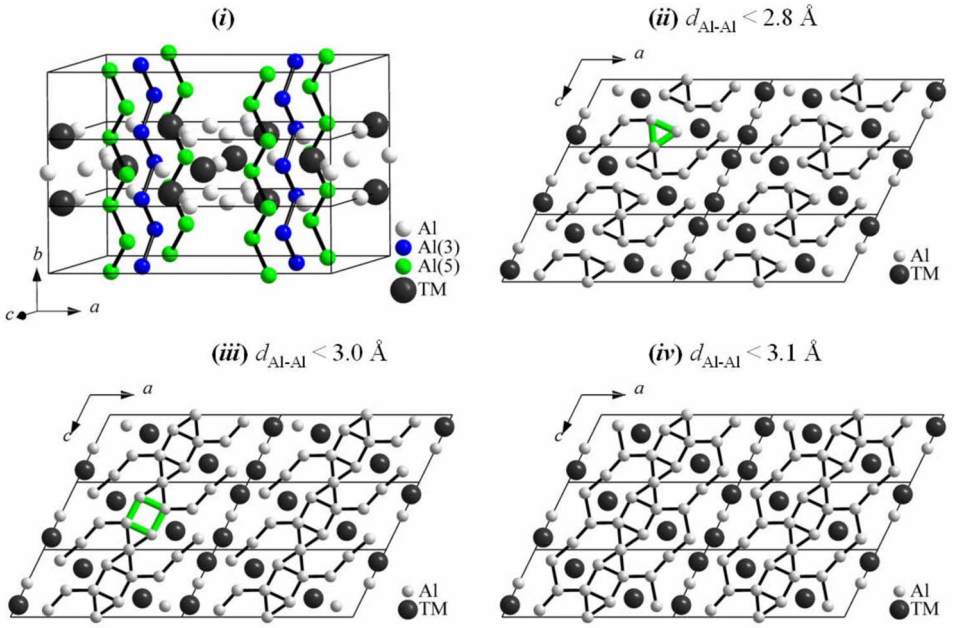

FIG. 10. (Color online) (i) Visualization of the Al-only atomic chains along b direction of the $Al_{13}TM_4$ structural model by Zhang *et al.* (Ref. 17). A "supercell," composed of three unit cells along b, is shown. There are two types of Al-only chains: Al(3)-Al(3)-Al(3)-⋯ with the interatomic distance $d_{\text{Al-Al}}=2.59$ Å (connected black small atoms, online blue colored) and Al(5)-Al(5)-Al(5)-⋯ with $d_{\text{Al-Al}}=2.67$ Å (connected gray small atoms, online green colored). In searching for the Al-only atomic chains within the (a,c) monoclinic plane, we find no connected chains along either a^* or c direction for the Al-Al distances $d_{\text{Al-Al}}<2.8$ Å [panel (ii), all interatomic distances smaller than 2.8 Å are drawn by solid lines]. By increasing allowed Al-Al distances to $d_{\text{Al-Al}}<3.0$ Å, connected Al-only chains appear along the c direction [panel (iii)] but not along the a^* (or a) direction. By increasing Al-Al distances further to $d_{\text{Al-Al}}<3.1$ Å [panel (iv)], there are still no connected chains along a^* (or a). Representative triangular and square configurations of Al atoms are highlighted with thicker lines (online green colored) in panels (ii) and (iii). These configurations can be viewed as planar closed current loops in the (a,c) plane for the magnetic field along direction, contributing to the Landau orbital diamagnetism of conduction electrons.

chains within the (a,c) monoclinic plane, we get the following result. Searching for connected Al chains with Al-Al distances $d_{\text{Al-Al}}<2.8$ Å, we find no connected Al-only chains along either c or a^* direction [panel (ii) of Fig. 10]. By increasing the allowed Al-Al distances to $d_{\text{Al-Al}}<3.0$ Å, we observe [panel (iii) of Fig. 10] that connected Al-only chains form along the c direction, whereas no connected chains can still be found along the a^* (or a) direction. By increasing Al-Al distances further to $d_{\text{Al-Al}}<3.1$ Å [panel (iv) of Fig. 10], there are still no connected chains along a^* (or a). These start to appear only by allowing very large distances $d_{\text{Al-Al}} \approx 3.4$ Å. Since the Al-Al distances are of crucial importance for the conductivity of a given chain (the smaller this distance, the lower the potential barrier to be crossed by an electron migrating from one to another Al atom in the chain), the chains with shorter Al-Al distances will be more conducting. The above analysis thus suggests the anisotropic conductivity of Y-Al-Ni-Co in the order $\sigma_b > \sigma_c > \sigma_{a^*}$ (or the resistivity $\rho_{a^*} > \rho_c > \rho_b$), in agreement with the experimental results displayed in Fig. 4. Since $d_{\text{Al-Al}}=2.59$ Å for the Al(3)-Al(3) chains along b is much shorter than the shortest $d_{\text{Al-Al}}$ for the c and a^* directions, even the inequality $\sigma_b \gg \sigma_c > \sigma_{a^*}$ can be qualitatively confirmed.

The anisotropy of the magnetic susceptibility can also be visualized from purely structural (and chemical) considerations. Figure 1 shows that the conduction-electron susceptibility of Y-Al-Ni-Co is diamagnetic for the magnetic field directed along b, whereas it is paramagnetic for the field lying in the (a,c) plane. Panel (ii) of Fig. 10 shows that the (a,c) plane contains triangles of Al atoms with short interatomic distances ($d_{\text{Al-Al}}=2.68$, 2.69, and 2.72 Å in a triangle). Applying magnetic field along the orthogonal b direction, these triangles represent closed planar current loops for the electron orbital circulation that contribute to the Landau diamagnetic susceptibility. Panel (iii) of Fig. 10 further shows that another type of an Al-only closed planar loop appears in the (a,c) plane with slightly larger Al-Al distances: these are squarelike parallelograms with interatomic distances $d_{\text{Al-Al}}=2.72$ and 2.86 Å, which again add to the Landau diamagnetic orbital circulation. These triangularlike and squarelike planar loops can be considered to be at the origin of the strong Landau diamagnetism for the field perpendicular to the (a,c) plane. For the field directed along the other two crystalline directions a^* and c, no Al-only loops can be found lying in the perpendicular (b,c) and (a^*,b) planes. Al-only triangles with relatively short interatomic distances can still be defined in the structure, but normals to their planes lie at high angles to the a^* and c directions, making these loops ineffective in contributing to the Landau diamagnetism when applying the field along these directions. The planar (a,c) structure of Y-Al-Ni-Co thus supports the strong Landau diamagnetic susceptibility for the field along b, whereas this contribution is weaker for the field along a^* and c. Consequently, Landau diamagnetic susceptibility wins over the Pauli paramagnetic susceptibility for the field along

b, making Y-Al-Ni-Co diamagnetic along this direction, whereas for the field along a^* and *c*, the Pauli susceptibility is stronger and Y-Al-Ni-Co becomes paramagnetic along these two directions.

V. SUMMARY AND CONCLUSIONS

We have investigated magnetic susceptibility, electrical resistivity, thermoelectric power, Hall coefficient, and thermal conductivity of the Y-Al-Ni-Co decagonal approximant. Our main objective was to find out whether there exists anisotropy of the investigated physical parameters when measured along the atomic planes, corresponding to the quasiperiodic planes in the related *d*-Al-Ni-Co quasicrystal, and perpendicular to the planes, corresponding to the periodic direction in *d*-QCs. Magnetic measurements have shown that the Curie magnetization of fixed paramagnetic ions is negligible, classifying Y-Al-Ni-Co among nonmagnetic alloys, but there exists significant anisotropy of the magnetization originating from conduction electrons. This magnetization is paramagnetic for the field lying within the (a,c) atomic planes, whereas it is diamagnetic for the field along the perpendicular *b* direction. This duality can be explained by considering anisotropic Landau diamagnetic orbital motion of conduction electrons. The structure of Y-Al-Ni-Co suggests the existence of planar current loops formed of closely spaced Al atoms within the (a,c) atomic planes, contributing to the Landau diamagnetic susceptibility for the field along *b*, whereas no such planar loops exist in the planes perpendicular to the a^* and *c* directions, making Landau orbital diamagnetism weaker for the field along these directions.

Electrical resistivity of Y-Al-Ni-Co is low in all crystalline directions, with the RT values in the range 25–81 $\mu\Omega$ cm. There exists significant anisotropy between the in-plane resistivity and the resistivity along the perpendicular *b* direction by a factor about 3, whereas the anisotropy between the two in-plane directions a^* and *c* is much smaller. The anisotropic resistivity appears in the order $\rho_{a^*} > \rho_c \gg \rho_b$, so that *b* direction is the most electrically conducting one. This order is confirmed theoretically by *ab initio* calculation of the resistivity ratios ρ_i/ρ_j along the investigated crystalline directions, using the Y-Al-Ni-Co-specific anisotropic Fermi surface. Considering that atomic chains made up of Al atoms only are the dominant conduction paths, analysis of the Y-Al-Ni-Co structure reveals that Al chains with the shortest interatomic distances propagate along the *b* direction, whereas the Al-Al distances are longer for the chains along *c* and even longer for the a^* (or *a*) direction. Structural analysis thus suggests the anisotropic resistivity in the same order as observed experimentally. The temperature-dependent resistivities for all directions show PTC, revealing that electron-phonon interaction provides the main scattering mechanism. This is different from the *d*-Al-Ni-Co quasicrystal, which shows PTC resistivity along the periodic direction but nonmetallic NTC resistivity for the in-plane directions. Comparison to $Al_4(Cr,Fe)$,[12] a member of the Al_4TM family of decagonal approximants with a giant unit cell shows that the anisotropic resistivity of $Al_4(Cr,Fe)$ is intermediate to the *d*-Al-Ni-Co quasicrystal and the Y-Al-Ni-Co approximant, showing nonmetallic resistivity for the in-plane directions [exhibiting a maximum in the $\rho(T)$ with NTC at high temperature and PTC at low temperature] and metallic PTC resistivity perpendicular to the atomic planes. Similarly to *d*-Al-Ni-Co and Y-Al-Ni-Co, the resistivity of $Al_4(Cr,Fe)$ is the lowest in the direction perpendicular to the atomic planes, which appears to be a common property of these stacked-layer compounds.

Thermopower of Y-Al-Ni-Co is negative, suggesting dominant electron-type carriers, and shows electron-phonon enhancement effect that results in a change in slope in the Seebeck coefficient $S(T)$ at about 70 K for all three investigated crystalline directions. Bare thermopower (in the absence of electron-phonon interactions) was extracted and its anisotropy was analyzed within the frame of the linearized Boltzmann transport equation. Assuming that the spectral conductivity does not exhibit sharp features in the vicinity of the Fermi level (supported theoretically by the smooth DOS around E_F) and the derivative of the spectral conductivity does not depend significantly on the crystalline direction, the magnitude of the thermopower in a given direction is then predominantly determined by the magnitude of the resistivity in that direction. This suggests anisotropic bare thermopowers in the same order as the anisotropic electrical resistivity, $|S^{\mathrm{bare}}_{a^*}/T| > |S^{\mathrm{bare}}_c/T| > |S^{\mathrm{bare}}_b/T|$, which was also observed experimentally.

Hall coefficient R_H of Y-Al-Ni-Co exhibits pronounced anisotropy, where the magnetic field in a given crystalline direction yields the same R_H for the current along the other two crystalline directions in the perpendicular plane. Two rather high positive values $R_H^{a^*}$ and R_H^c for the field lying in the (a,c) atomic plane and the almost zero value of R_H^b for the field along the perpendicular *b* direction reflect strong anisotropy of the Fermi surface that consists mostly of holelike parts, whereas electronlike and holelike parts are of comparable importance for the field perpendicular to the (a,c) plane. At the same time, negative thermopower suggests that the Fermi surface is mostly electronlike. While this apparent contradiction can be in principle resolved by considering direction-dependent details of the anisotropic Fermi surface (but the analysis was not preformed here), opposite signs $S<0$ and $R_H>0$ were also reported for the high-T_c cuprates and the explanation was given in terms of an unusual electronic state in which the Hall (cyclotron) mass parallel to the Fermi surface is holelike (<0) but the transport mass perpendicular to it is electronlike (>0). The applicability of this hypothesis to Y-Al-Ni-Co remains a theoretical challenge. There is complete analogy between the R_H anisotropy of Y-Al-Ni-Co and *d*-QCs, where, in the latter, $R_H > 0$ for the field lying in the quasiperiodic plane (corresponding to the in-plane coefficients $R_H^{a^*}, R_H^c > 0$ of Y-Al-Ni-Co), whereas R_H changes sign to negative for the field along the periodic direction (corresponding to $R_H^b \approx 0$ of Y-Al-Ni-Co).

Anisotropic thermal conductivities appear in the order $\kappa^b > \kappa^c > \kappa^{a^*}$ and the same order applies to their electronic part, $\kappa^b_{\mathrm{el}} > \kappa^c_{\mathrm{el}} > \kappa^{a^*}_{\mathrm{el}}$, estimated from the Wiedemann-Franz law. This order is identical to the order in which the aniso-

tropic electrical conductivities appear. The anisotropic phononic thermal conductivity again appears in the same order, $\kappa_{\mathrm{ph}}^{b} > \kappa_{\mathrm{ph}}^{c} > \kappa_{\mathrm{ph}}^{a^*}$. For all directions, κ_{ph}'s show a typical phonon umklapp maximum at about 40 K. Y-Al-Ni-Co is thus the best conductor, both electrical and thermal, along the b direction perpendicular to the atomic planes, whereas both conductivities are smaller in the (a,c) atomic plane.

The above results show good analogy between the anisotropic physical properties of the quasiperiodic d-Al-Ni-Co quasicrystal on one hand and the periodic Y-Al-Ni-Co and $Al_4(Cr,Fe)$ decagonal approximants on the other hand. This suggests that long-range quasiperiodicity of the structure is of marginal importance (if it is of any at all) for the anisotropy, which originates from the complex local atomic order on the scale of nearest-neighbor atoms.

ACKNOWLEDGMENTS

This work was done within the activities of the Sixth Framework EU Network of Excellence, "Complex Metallic Alloys" (Contract No. NMP3-CT-2005-500140). A.S. acknowledges support of the Ministry of Science, Education and Sports of the Republic of Croatia through the Research Project No. 035–0352826-2848. O.S.B. acknowledges useful discussion with E. Tutiš.

[1] T. Shibuya, T. Hashimoto, and S. Takeuchi, J. Phys. Soc. Jpn. **59**, 1917 (1990).
[2] S. Martin, A. F. Hebard, A. R. Kortan, and F. A. Thiel, Phys. Rev. Lett. **67**, 719 (1991).
[3] Wang Yun-ping and Zhang Dian-lin, Phys. Rev. B **49**, 13204 (1994).
[4] Lin Shu-yuan, Wang Xue-mei, Lu Li, Zhang Dian-lin, L. X. He, and K. X. Kuo, Phys. Rev. B **41**, 9625 (1990).
[5] Zhang Dian-lin, Lu Li, Wang Xue-mei, Lin Shu-yuan, L. X. He, and K. H. Kuo, Phys. Rev. B **41**, 8557 (1990).
[6] Wang Yun-ping, Zhang Dian-lin, and L. F. Chen, Phys. Rev. B **48**, 10542 (1993).
[7] Zhang Dian-lin, Cao Shao-chun, Wang Yun-ping, Lu Li, Wang Xue-mei, X. L. Ma, and K. H. Kuo, Phys. Rev. Lett. **66**, 2778 (1991).
[8] K. Edagawa, M. A. Chernikov, A. D. Bianchi, E. Felder, U. Gubler, and H. R. Ott, Phys. Rev. Lett. **77**, 1071 (1996).
[9] D. N. Basov, T. Timusk, F. Barakat, J. Greedan, and B. Grushko, Phys. Rev. Lett. **72**, 1937 (1994).
[10] M. Krajčí and J. Hafner, Phys. Rev. B **58**, 5378 (1998).
[11] G. Trambly de Laissardière and T. Fujiwara, Phys. Rev. B **50**, 9843 (1994).
[12] J. Dolinšek, P. Jeglič, M. Komelj, S. Vrtnik, A. Smontara, I. Smiljanić, A. Bilušić, J. Ivkov, D. Stanić, E. S. Zijlstra, B. Bauer, and P. Gille, Phys. Rev. B **76**, 174207 (2007).
[13] J. Dolinšek, S. Vrtnik, A. Smontara, M. Jagodič, Z. Jagličić, B. Bauer, and P. Gille, Philos. Mag. (to be published).
[14] D. W. Deng, Z. M. Mo, and K. H. Kuo, J. Phys.: Condens. Matter **16**, 2283 (2004).
[15] G. Trambly de Laissardière, J.-P. Julien, and D. Mayou, Phys. Rev. Lett. **97**, 026601 (2006).
[16] P. Volkov and S. J. Poon, Phys. Rev. B **52**, 12685 (1995).
[17] B. Zhang, V. Gramlich, and W. Steurer, Z. Kristallogr. **210**, 498 (1995).
[18] R. C. Hudd and W. H. Taylor, Acta Crystallogr. **15**, 441 (1962).
[19] J. Grin, U. Burkhardt, M. Ellner, and K. Peters, J. Alloys Compd. **206**, 243 (1994).
[20] J. Grin, U. Burkhardt, M. Ellner, and K. Peters, Z. Kristallogr. **209**, 479 (1994).
[21] L.-E. Edshammar, Acta Chem. Scand. (1947-1973) **18**, 2294 (1964).
[22] L.-E. Edshammar, Acta Chem. Scand. (1947-1973) **19**, 2124 (1965).
[23] Z. A. Chaudhury and C. Suryanarayana, J. Less-Common Met. **91**, 181 (1983).
[24] S. Kek, Ph.D. thesis, University of Stuttgart, 1991.
[25] W. Steurer, T. Haibach, B. Zhang, S. Kek, and R. Lück, Acta Crystallogr., Sect. B: Struct. Sci. **49**, 661 (1993).
[26] Y. Yamada, Y. Yokoyama, K. Matono, and K. Fukaura, Jpn. J. Appl. Phys., Part 1 **38**, 52 (1999).
[27] J. T. Markert, J. L. Cobb, W. D. Bruton, A. K. Bhatnagar, D. G. Naugle, and A. R. Kortan, J. Appl. Phys. **76**, 6110 (1994).
[28] P. W. Selwood, *Magnetochemistry* (Interscience, New York, 1956), p. 78.
[29] F. E. Mabbs and D. J. Machin, *Magnetism and Transition Metal Complexes* (Chapman and Hall, London, 1973), p. 7.
[30] P. Jeglič and J. Dolinšek, Phys. Rev. B **71**, 014204 (2005).
[31] A. Kobayashi, S. Matsuo, T. Ishimasa, and H. Nakano, J. Phys.: Condens. Matter **9**, 3205 (1997).
[32] J. Dolinšek, T. Apih, P. Jeglič, I. Smiljanić, A. Bilušić, Ž. Bihar, A. Smontara, Z. Jagličić, M. Heggen, and M. Feuerbacher, Intermetallics **15**, 1367 (2007).
[33] A. Smontara, I. Smiljanić, A. Bilušić, Z. Jagličić, M. Klanjšek, S. Roitsch, J. Dolinšek, and M. Feuerbacher, J. Alloys Compd. **430**, 29 (2007).
[34] See, e.g., U. Mizutani, *Introduction to the Electron Theory of Metals* (Cambridge University Press, Cambridge, 2001), p. 268.
[35] See, for a review, U. Mizutani (Ref. 34), Chap. 10.
[36] P. Blaha, K. Schwarz, P. Sorantin, and S. B. Trickey, Comput. Phys. Commun. **59**, 399 (1990).
[37] E. Wimmer, H. Krakauer, M. Weinert, and A. J. Freeman, Phys. Rev. B **24**, 864 (1981).
[38] P. E. Blöchl, O. Jepsen, and O. K. Andersen, Phys. Rev. B **49**, 16223 (1994).
[39] A. Kokalj, Comput. Mater. Sci. **28**, 155 (2003); Code available from (http://www. xcrysden.org).
[40] G. Lehmann and M. Taut, Phys. Status Solidi B **54**, 469 (1972).
[41] A. B. Kaiser, Phys. Rev. B **29**, 7088 (1984).
[42] Lin Shuyuan, Li Guohong, and Zhang Dianlin, Phys. Rev. Lett. **77**, 1998 (1996).
[43] Y. Kubo, Phys. Rev. B **50**, 3181 (1994).